

Nanoparticles induce dermal and intestinal innate immune system responses in zebrafish embryos

Nadja R. Brun^{1,2*}, Bjørn E.V. Koch³, Mónica Varela³, Willie J.G.M. Peijnenburg^{1,4}, Herman P. Spaink³, Martina G. Vijver¹

¹Institute of Environmental Sciences (CML), Leiden University, Leiden, The Netherlands

²Department of Biology, Woods Hole Oceanographic Institution, Woods Hole MA, USA

³Institute of Biology, Leiden University, Leiden, The Netherlands

⁴National Institute of Public Health and the Environment (RIVM), Center for Safety of Substances and Products, Bilthoven, The Netherlands

*Corresponding author

n.r.brun@cml.leidenuniv.nl

Keywords

copper nanoparticles, polystyrene nanoparticles, inflammation, neuromasts, intestine

Environmental Significance

Increasing our understanding of how nanoparticles affect organisms is essential to predict and mitigate environmental threats, yet to date little is known about their potential to affect immune systems in aquatic organisms. In this work, primary sites of metallic and plastic nanoparticle accumulation and their potential to induce an inflammatory response are explored in zebrafish embryo. This study provides initial evidence that nanoparticles accumulate on the external and internal epithelium, and can elicit transcription of pro-inflammatory cytokines in zebrafish embryos. This can potentially be used as a building block in developing adverse outcome pathways for nanoparticles in ecological risk assessment.

37 **Abstract**

38 Major molecular mechanisms that underpin the toxicity of nanoparticles (NPs) are the formation
39 of reactive oxygen species and the induction of inflammation. The latter is frequently observed
40 *in vitro* and in mammalian organisms, yet in aquatic organisms, such NP-induced inflammatory
41 responses remain largely unexplored. Zebrafish offer a wide range of molecular tools to investi-
42 gate immune responses in an aquatic organism, and were therefore used here to describe how
43 copper (Cu) NPs (25 nm; 1 mg L⁻¹) and soluble Cu as well as polystyrene (PS) NPs (25 nm; 10
44 mg L⁻¹) induce innate immune responses, focussing on the skin cells and the intestine as likely
45 organs of interaction. mRNA expression of the immune responsive genes *interleukin 1 beta*
46 (*il1β*) and *immunoresponsive gene 1-like (irg1)* of CuNP exposed embryos was observed to be
47 weaker in the intestinal tissue compared to the rest of the body, indicating a strong outer epithe-
48 lium response. Specifically, NPs were observed to accumulate in the cavities of lateral neuro-
49 masts in the skin, which coincided with an increased local expression of *il1β*. Exposure to
50 CuNPs triggered the strongest transcriptional changes in pro-inflammatory-related genes and
51 was also observed to increase migration of neutrophils in the tail, indicating a NP-specific in-
52 flammatory response. This is the first *in vivo* evidence for waterborne NP exposure triggering
53 alterations of immune system regulating genes in the skin and intestines of zebrafish embryos.
54 The observed molecular responses have the potential to be linked to adverse effects at higher
55 levels of biological organization and hence might offer screening purposes in nanotoxicology or
56 building blocks for adverse outcome pathways.

57

58 Introduction

59 Nanoparticles (NPs) pose a potential risk to ecosystems and the organisms living therein due to
60 widespread use in medical and consumer products, and subsequent gradual release into the
61 environment. An increasing number of studies are therefore aimed at understanding of uptake
62 routes, bioaccumulation potential, and mode of actions of NPs. However, formulating a general
63 framework for risk assessments is currently hampered by the plethora of variables affecting NP
64 bioavailability and toxicity, including different core compositions, shapes, sizes and surface
65 modifications.¹ An emerging approach in risk assessment is therefore, to unravel shared molec-
66 ular responses caused by exposure as this can be linked to adverse effects at higher levels of
67 biological organization, a concept known as adverse outcome pathways (AOPs).²

68 Two major molecular pathways are commonly affected by exposure to particles in the
69 nanometer range: oxidative stress and inflammation. Generation of reactive oxygen species
70 (ROS) fuelled by NPs or metal ions dissolved from NPs is a key mechanism of NP toxicity that
71 is frequently observed and is currently the best-understood mechanism,³⁻⁵ in which the for-
72 mation of highly reactive oxygen radicals can disturb mitochondrial function ultimately leading to
73 apoptosis.^{6,7} However, metals and NPs are also recognized as a potent inducer of immune and
74 inflammatory responses.⁸ Epithelial and mucosal linings are major components of the innate im-
75 mune system and are the site where NPs may be recognized as pathogens by the Toll-like re-
76 ceptors, triggering innate immune responses in the organism and leading to induction of pro-in-
77 flammatory genes such as interleukins, cytokines, and chemokines.⁹ The organism's response
78 culminates in recruiting phagocytic cells (neutrophils and macrophages) to the site of infection
79 or injury. This suggests that NP-induced inflammation might also serve as a sensitive molecular
80 response, and hence it is key to identify primary sites of induction and relative sensitivity.

81 In aquatic organisms, it is widely accepted that the NPs first target the outer skin and the
82 intestine¹⁰, which correlates with the primary sites where the innate immune system can be acti-
83 vated. On the external epithelial membranes of fish, NPs can interfere with the lateral line sys-
84 tem, inducing oxidative stress or apoptotic cell death in neuromasts, ultimately leading to a re-
85 duction of functional neuromasts and attenuated orientation within a current.¹¹⁻¹³ Although lat-
86 eral line neuromasts are used for screening purposes to identify immunomodulatory com-
87 pounds, NPs have not yet been assessed for this activity. In intestines of juvenile fish, an im-
88 mune response after NP exposure was detected by increased mRNA levels of pro-inflammatory
89 related genes after copper (Cu) NPs exposure.¹⁴ Moreover, the effect was more pronounced for
90 the NP than for the soluble copper exposure. In zebrafish embryos, despite being a widely used
91 organism to screen for NP toxicity or investigate immune responses, target sites of NPs have
92 not yet been explored for such responses. Whole embryo assessment revealed that gold NPs
93 (1.5 nm) alter genes involved in inflammatory pathways after waterborne exposure of dechori-
94 onated embryos¹⁵ and injected silica NPs (62 nm) lead to neutrophil-mediated cardiac inflamma-
95 tion.¹⁶ Innate immune responses in early life stages of fish triggered by NPs is thus conceivable,
96 however, the assessment and localization of inflammation as a molecular key event after water-
97 borne exposure of NPs remains largely unexplored.

98 Zebrafish embryos are due to their transparency a suitable living system to study the
99 dermal and intestinal epithelium as potential sites of action of NPs. More importantly, the
100 zebrafish embryo is a widely used model organism that is well established in immunology and
101 allows for the tracking of fluorescently labeled compounds as well as several key immune
102 responsive genes and cells in different organs.¹⁷ Our aim was to use this aquatic model organ-
103 ism to investigate the two putative sites of NP accumulation, the skin and the intestine, and to
104 compare their potential to elicit an inflammatory response. To disentangle the NP contribution,
105 an inert polystyrene NP (PSNP) and a metallic NP (CuNP), as well as the dissolved metal frac-
106 tion released from the metal NP, were assessed. While Cu is a metal well-recognized for its

107 potential to elicit an inflammatory response, the toxic mechanism of PSNP remains largely un-
108 explored. An environmentally relevant concentration of fulvic acid was added to stabilize metal
109 particle aggregation, complex toxic Cu^{2+} , and mimic environmentally relevant conditions. The
110 dosage of NPs was based on no observed adverse effects for malformation. Immune responses
111 were subsequently assessed with qPCR and *in situ* hybridization targeting genes from the in-
112 nate immune responses in whole body, intestine, and body without intestine samples and with
113 transgenic zebrafish lines expressing green fluorescent proteins (GFP) under interleukin 1 beta
114 (*il1 β*), tumor necrosis factor alpha (*tnfa*), neutrophil-specific (myeloperoxidase, *mpx*) and macro-
115 phage-specific (*mpeg*) promoter.

116 **Materials and Methods**

117 **Materials.** CuNPs (chemical formula: Cu, with a specific surface area of 30–50m²/g, a purity of
118 95.5% and a density of 8.92 g/cm³) with a nominal size of 25 nm were purchased as dry powder
119 from IoLiTec, Inc. (Germany) and copper(II) nitrate ($\text{Cu}(\text{NO}_3)_2$ from Sigma-Aldrich (The Nether-
120 lands) was used as dissolved metal control. Fluorescent polystyrene particles (PSNP; 25 nm,
121 ThermoFisher Scientific, U.S.) were used as an inert NP and to track target organs of particles.
122 The Suwannee River humic acid (SRHA) standard containing 15% fulvic acid and 85% humic
123 acid (International Humic Substances Society, Atlanta, Georgia) was used as a surrogate for or-
124 ganic matter.

125 **SRHA, Cu, and polystyrene nanoparticle characterization.** A stock solution of 1000 mg L⁻¹
126 SRHA in egg water (60 mg L⁻¹ InstantOcean Sea Salt, Sera Marin) was prepared according to
127 Wang et al. (2015)¹⁸. In pre-experiments, the nominal concentration of 30 mg L⁻¹ SRHA was de-
128 termined to decrease particle aggregation (**Figure S1a, b** in Electronic Supplementary Infor-
129 mation, ESI) and not to influence normal embryo development (data not shown). The total
130 amount of organic carbon (TOC) in exposure media was analyzed by TOC analysis (Thermo
131 Hiper; ThermoFisher Scientific, U.S.).

132 Prior to use, both nanoparticles were characterized by size, shape, surface charge, and
133 aggregation. Transmission electron microscopy (TEM; JEOL 1010, JEOL Ltd., Japan) was used
134 to characterize the size and shape of the NPs after 1 hour of incubation in egg water. Size distri-
135 bution and zeta potential of all exposure samples were measured directly after preparation (0 h)
136 and after 24 h incubation by dynamic light scattering (DLS; Zetasizer, Malvern Instruments, UK).
137 Three independent measurements were performed, each consisting of three repeated measure-
138 ments. Dissolved Cu concentration from CuNP exposure suspensions was measured over time
139 (0 h, 24 h, and 48 h) using flame atomic absorption spectroscopy (AAS; Perkin Elmer 1100B,
140 The Netherlands) by collecting samples from the suspension and the supernatant (after centrifu-
141 gation for 20 min at 14680 rpm at 4 °C) and acidifying it in 10% HNO_3 overnight at room temper-
142 ature. Centrifugation at this speed was previously shown to efficiently remove CuNPs from sus-
143 pension.¹⁹ The measurements were carried out in triplicate. The percentage of dissolution of the
144 CuNPs was then calculated as the percentage of the total copper concentrations. Furthermore,
145 the amount of dissolved Cu in mg L⁻¹ was used to derive the corresponding copper nitrate con-
146 centration. In order to achieve a copper nitrate stock solution of a known measured concentra-
147 tion, a stock solution of 1 mg mL⁻¹ copper nitrate in Milli-Q was prepared. Thereof, serial dilu-
148 tions ranging from 0.4 to 5 mg L⁻¹ were prepared and measured by AAS to calculate a linear
149 standard curve of nominal versus measured copper nitrate concentration. The equation derived
150 from linear regression analysis allowed the use of a copper nitrate concentration corresponding
151 to the measured dissolved copper from CuNP.

152 **Modelling of metal speciation.** Visual MINTEQ (Ver 3.1)²⁰ was used to model the speciation of
153 0.59 mg L⁻¹ free copper (released from 1 mg L⁻¹ CuNP or added as $\text{Cu}(\text{NO}_3)_2$) in egg water at
154 pH 7.0. The NICA-Donnan model with a specification of 15% solid fulvic acid and 85% humic

155 acid at a concentration of 12.9 mg L⁻¹ (according to mean measured concentrations) was ap-
156 plied to calculate the binding of metals by SRHA.

157 **Embryo exposure.** Zebrafish were handled in compliance with animal welfare regulations and
158 maintained according to standard protocols (<http://ZFIn.org>). The culture was approved by the
159 local animal welfare committee (DEC) of the University of Leiden and all protocols adhered to
160 the international guidelines specified by EU Animal Protection Directive 2010/63/EU. Zebrafish
161 eggs were obtained from mixed egg clutches from wildtype ABxTL strain, *Tg(mpx:eGFP)*²¹,
162 *Tg(mpeg1:eGFP)*²², *Tg(il1b:eGFP-F)*²³, and *Tg(tnfa:eGFP-F)*²⁴ strain. Fertilized eggs were dis-
163 tributed in 6-well plates (20 embryos per well) with 6 ml of exposure solution: control (egg wa-
164 ter), control supplemented with SRHA, 0.1 mg L⁻¹ CuNP and corresponding copper nitrate con-
165 centration, 1 mg L⁻¹ CuNP and corresponding copper nitrate concentration, and 10 mg L⁻¹ PSNP
166 with 5 replicates in each group. The concentration of NPs was based on no observed adverse
167 effects for malformation derived from pilot studies. The CuNP at a final concentration of 0.1 and
168 1 mg L⁻¹ were dispersed in egg water supplemented with SRHA and the PSNP were dispersed
169 in egg water only. All exposure media were sonicated in an ultrasonic water bath (USC200T,
170 VWR, Amsterdam, The Netherlands) for 5 min prior to exposure.

171 For the copper uptake experiment and assessment of morphological endpoints (hatching
172 success, developmental anomalies, size, and mortality), ABxTL embryos were exposed in 6-
173 well plates (10 embryos per well, 1 wells per exposure group) from 0 to 120 hpf. Hatching suc-
174 cess, developmental anomalies, and mortality was assessed from five independent egg
175 clutches. Exposure medium and egg water were replaced daily and embryos were screened for
176 morphological endpoints using a Leica stereomicroscope (M165 C, Switzerland). At 72 hpf 10
177 ABxTL embryos per exposure group were sampled for quantification of copper concentrations.
178 At the end of exposure at 120 hpf, 10 hatched ABxTL embryos were imaged for size measure-
179 ment using the stereomicroscope equipped with a camera (DFC 420) and 5 embryos thereof
180 sampled for copper concentration measurement. The larval size was determined using Im-
181 ageJ²⁵.

182 For RNA extraction and *in situ* hybridization, hatched embryos were exposed from 72 to
183 120 hpf in 6-well plates with one exposure medium replacement. At the end of exposure at 120
184 hpf, 15 embryos per replicate were snap frozen in liquid nitrogen and sampled for RNA extrac-
185 tion. For live imaging of immune responses, a short-term exposure of 24 h and a lower CuNP
186 (0.1 mg L⁻¹) concentration was chosen in addition to the exposure above. A shorter exposure
187 time enables the detection of early inflammatory responses and a lower CuNP concentration of
188 0.1 mg L⁻¹ was chosen, as 1 mg L⁻¹ copper could slow down development.

189 **Extraction of the intestine.** For organ-specific expression analysis using qPCR, the intestine of
190 120 hpf embryos was extracted from anesthetized embryos by fixing the anterior part with insect
191 needles and pulling on the jaw using forceps. The tissues were directly placed into Trizol for
192 subsequent RNA extraction. Intestines or bodies without intestine of 10 embryos per group were
193 pooled to one replicate. Three replicates per group (control and 1 mg L⁻¹ CuNP) were prepared.
194 Genes of interest with local expression in intestinal tissue were *il1β*, *irg1l*, and *tnfa*.

195 **Quantification of copper concentration in zebrafish embryos.** For total Cu quantification in
196 zebrafish embryos, 5 embryos per replicate (n = 3) were collected at 72 hpf and 120 hpf and
197 dechorionated if not hatched. Only viable embryos with no morphological malformations were
198 chosen. Embryos were washed three times with Milli-Q water supplemented with 1 mM EDTA.
199 Once rinsed, embryos were transferred into Eppendorf tubes and excess liquid was removed.
200 Samples were digested in 300 μL aqua regia (HNO₃:HCl; 1:3) overnight and subsequently
201 heated to 70 °C to evaporate all liquid. The residue was dissolved in 0,1 n HNO₃ in super-
202 demineralized water and measured by Graphite Furnace Atomic Absorption Spectrometry (GF-
203 AAS; Perkin Elmer, The Netherlands).

204 **RNA isolation, cDNA synthesis, and expression analyses.** Total RNA (1 µg) was extracted
205 using Trizol (Invitrogen) according to manufacturer's protocol, purified on RNeasy MinElute
206 Cleanup columns (Qiagen, The Netherlands) and quantified using a NanoDrop ND-1000 Spec-
207 trophotometer (Nanodrop Technologies Inc., U.S.). The first strand cDNA was synthesized
208 thereof using the Omniscript™ Reverse Transcriptase kit (Qiagen, The Netherlands), Oligo-dT
209 primers (Qiagen), and RNase inhibitor (Promega). cDNAs were then diluted 5 times and reverse
210 transcription-quantitative polymerase chain reaction (RT-qPCR) was conducted with gene-spe-
211 cific primer pairs (**Table S1, ESI**) mixed with SYBR Green (iQ supermix, Qiagen, The Nether-
212 lands). The samples were denatured for 5 min at 95 °C and then amplified using 40 cycles of 15
213 s at 95°C and 45 s at 58 °C or 60 °C (depending on transcript target), respectively, followed by
214 quantitation using a melting curve analysis post run. Amplification and quantification were done
215 with the CFX96 Biorad system and was run with five biological replicates (or three for intestine
216 and body without intestine samples) and two technical duplicates. Fold induction was calculated
217 by normalizing C_T values of the target gene to the C_T value of the housekeeping gene β -actin
218 ($=\Delta C_T$) and then normalized to the untreated control (ΔC_T untreated – ΔC_T treated).

219 **In situ hybridization.** Wild-type zebrafish embryos (ABxTL strain) were raised in 0.003% 1-
220 phenyl-2-thiourea (PTU; Sigma-Aldrich, The Netherlands) no later than 24 hpf to prevent pig-
221 mentation. Hatched embryos were exposed to 10 mg L⁻¹ PSNP, 1 mg L⁻¹ CuNP and corre-
222 sponding copper nitrate concentration from 72 to 120 hpf with one medium exchange after 24 h.
223 Embryos were anesthetized with 200 µg mL⁻¹ 3-amino-benzoic acid (Tricaine; Sigma-Aldrich) on
224 ice and fixed in 4% paraformaldehyde. Whole-mount *in situ* hybridization was performed using a
225 standard protocol²⁶. *Irg1l* was tested by two non-overlapping digoxigenin-labeled anti-sense
226 RNA probes produced by PCR amplification and *in vitro* transcription, using the approach previ-
227 ously described²⁷. Primer sequences (5'-3'): probe #1 F: CACATGTATGCTTCTGAC-
228 GACATCAG, probe #1 R: AAGCCCGCTTGGTTTGCTGTTGCTG, probe #2 F: GGGCATT-
229 GAAATACAAGGCCGACTG, probe #2 R: AGATTGTGTTGCAGCATTAGCCATTGG.

230 **Intravenous microinjection.** Wild-type zebrafish embryos were treated with PTU from 24 hpf
231 onwards. Embryos were manually dechorionated at 24 hpf and after anesthetizing the embryos,
232 injection was performed at 30 hpf in the blood island with 1 nl of MilliQ (control), 0.5 mg L⁻¹
233 CuNP in MilliQ, or 1 mg L⁻¹ PSNP in MilliQ using a Femtojet injector (Eppendorf). All injection
234 solutions contained 1% phenol red and were sonicated before injection. 24 h later, whole body
235 and tail imaging were performed and 15 embryos per replicate snap-frozen for subsequent RNA
236 extraction and qPCR.

237 **Live imaging of immune responses and NP target organs.** Distribution of neutrophils and
238 macrophages were visualized using the transgenic zebrafish reporter lines for neutrophils
239 *Tg(mpx:eGFP)* and macrophages *Tg(mpeg1:eGFP)* after exposure to 0.1 mg L⁻¹ CuNP and 10
240 mg L⁻¹ PSNP from 96-120 hpf. The activation of *il1β* was visualized using the *Tg(il1b:eGFP-F)*
241 line. Embryos used for stereo fluorescence imaging were kept in egg water containing 0.0003%
242 PTU to prevent pigmentation. Embryos were anesthetized in tricaine for imaging with a Leica
243 stereo fluorescence microscope (M205 FA) equipped with a digital camera (DFC 345 FX). Each
244 image contains 3 channels: bright field, fluorescent green (GFPgreen), and fluorescent red
245 (DRSred). In order to visualize the expression of *il1β* and *tnfa* in the neuromasts and skin cells,
246 *Tg(il1b:eGFP-F)* and *Tg(tnfa:eGFP-F)* were exposed as described above but without PTU and
247 then fixed in 4% PFA overnight before being transferred in TBST and subsequent imaging un-
248 der a Leica SPE confocal using 40x water objective.

249 **Statistical Analyses.** The data were graphically illustrated with GraphPad Prism 6 (GraphPad
250 Software, U.S.). Variance homogeneity of the data was assessed with Bartlett's test. Fold
251 changes were log₂ transformed. Significant differences between treatments were assessed by
252 one-way ANOVA followed by a Bonferroni multiple comparison test ($p \leq 0.05$) to compare treat-
253 ment means with respective controls. All measurements (TEM, DLS, TOC, AAS) were

254 conducted in triplicates ($n = 3$) except for morphological endpoints including hatching success,
255 developmental anomalies, and mortality (5 independent experiments with 10 embryos each; $n =$
256 5), size measurement ($n = 10$), qPCR ($n = 3-5$), imaging of *in situ*, microinjections, and reporter
257 lines ($n = 10$) with one representative picture depicted. Results are expressed as means \pm
258 standard deviation of the mean (SD). Differences were considered statistically significant at $p \leq$
259 0.05.

260 Results

261 **Nanoparticle characterization.** The initial particle size of both nanoparticles, CuNP and PSNP,
262 was confirmed to be approximately 25 nm as visualized using TEM (**Figure 1a**). Imaging re-
263 vealed that both particles had a roughly spherical shape. The TEM images revealed single parti-
264 cles and agglomerates for both particles. It should be noted that the picture in Figure 1a does
265 not reflect a representative cluster size but the picture with the best contrast. Once dispersed in
266 egg water, CuNP agglomerated immediately to clusters with an average hydrodynamic diameter
267 of 291 ± 30 nm and to even bigger clusters of 375 ± 36 nm after 24 h. PSNP, on the other hand,
268 remained stable over time with an average size in the medium of 19.3 ± 0.6 nm after 0 h or 18.8
269 ± 0.9 nm after 24 h, respectively (**Figure 1b**). The zeta potential of both particles remained be-
270 tween -20 and -30 mV over time (**Figure 1c**), indicating a continuous negative surface charge
271 and thus repulsion forces keeping the particles in a rather stable suspension. Nevertheless, the
272 CuNP clustered to agglomerates of various sizes.

273 The major impact of SRHA on CuNP suspension characteristics is the complexation of
274 the free copper ions. The total concentration of Cu^{2+} is reduced from 49.4 % in pure egg water
275 to 9.2 % in egg water with SRHA as calculated by Visual Minteq (**Table S2**, ESI). The addition
276 of 30 mg L^{-1} SRHA to egg water resulted in a mean concentration of $12.9 \pm 0.4 \text{ mg L}^{-1}$ TOC
277 (**Figure S2**, ESI). Deviations between measured concentrations and nominal concentration can
278 be attributed to the filtration step while preparing the SRHA stock solution. Although the addition
279 of SRHA to the CuNP suspension did not prevent clustering of particles, the distribution of the
280 hydrodynamic diameters was smaller and more uniform than without addition of SRHA (**Figure**
281 **1b**, **Figure S1a**, ESI). Moreover, the zeta potential remained more stable over time with SRHA,
282 whereas it was closer to zero after 24 h in egg water only (**Figure S1b**, ESI). Taken together it
283 can be concluded that the physicochemical characteristics of CuNP are altered towards a more
284 stable colloidal suspension and free Cu^{2+} were significantly reduced upon addition of SRHA.

285 The total amount of copper measured in the exposure medium after 24 h was $0.08 \pm$
286 0.02 mg L^{-1} for 0.1 mg L^{-1} nominal CuNP (**Figure S1c**, ESI) and $0.73 \pm 0.11 \text{ mg L}^{-1}$ for 1 mg L^{-1}
287 nominal CuNP (**Figure S1d**, SI). Dissolution of free copper species after 24 h from 0.1 mg L^{-1}
288 CuNP was $0.06 \pm 0.01 \text{ mg L}^{-1}$ and for 1 mg L^{-1} CuNP it was $0.59 \pm 0.09 \text{ mg L}^{-1}$. The release of
289 free copper species slightly increased over the first 24 h and remained stable afterward (**Figure**
290 **1d**, **d**, SI). The concentration of $\text{Cu}(\text{NO}_3)_2$ was corresponding to the soluble copper fraction in
291 the CuNP solution as shown in **Figure S1d** in the ESI.

292 **Uptake and effects during embryo development.** During the first 72 h, zebrafish embryos de-
293 velop within a chorion. Embryos exposed to CuNP and corresponding $\text{Cu}(\text{NO}_3)_2$ from 0-72 hpf
294 showed the highest copper concentration in the chorion whereas in the embryo itself no in-
295 creased copper concentration was measured in comparison to the control (**Figure 2a**). This in-
296 dicates the chorions protective role in the first 72 h and thus in subsequent experiments em-
297 bryos were exposed after hatching. Remarkably, copper concentrations in chorions of CuNP ex-
298 posed embryos were significantly higher than in $\text{Cu}(\text{NO}_3)_2$ exposed embryos, suggesting an
299 increased accumulation of CuNP on the chorion (**Figure 2a**). Likewise, after hatching (at 120
300 hpf) CuNP exposed embryos contain more copper than $\text{Cu}(\text{NO}_3)_2$ exposed embryos (**Figure 2b**).
301 Both the intestine and the skin epithelium seem to be surface areas with increased NP accumu-
302 lation as PSNP accumulate in the gastrointestinal tract as well as in the cavity of lateral line

303 neuromasts and on the tail epithelium (**Figure 3**). Methods to visualize sites of accumulation
304 used for CuNP and PSNP were not interchangeable, however, it is likely that both CuNP and
305 PSNP accumulate on the outer epidermis and in the gastrointestinal tract.

306 Both CuNP and Cu(NO₃)₂ had similar effects on measured morphological endpoints.
307 Both delayed the hatching success to the same extent (**Figure 2c**). At 120 hpf, all embryos of
308 both exposure groups were hatched, nonetheless, an equally impaired growth in both exposure
309 groups was measured (**Figure 2d**). PSNP exposure had no effect on the measured endpoints
310 of embryo development.

311 **Inflammatory responses.** The inflammatory responses of embryos were assessed after water-
312 borne exposure and injection. Further, the transcriptional alterations of waterborne exposed em-
313 bryos were assessed in whole embryos and in intestinal tissue.

314 After waterborne exposure, whole embryo mRNA of pro-inflammatory cytokines (*irg1l*,
315 *il1β*, and *tnfa*) were significantly altered after exposure to 10 mg L⁻¹ PSNP and the chemokine
316 *ccl20a* after exposure to PSNP, 1 mg L⁻¹ CuNP, and 0.59 mg L⁻¹ Cu(NO₃)₂ (**Figure S3a, ESI**).
317 Contrariwise, only for CuNP, an increased the number of neutrophils in the tail area was
318 counted, although not significantly (**Figure S3b, ESI**). Whole body and tail imaging of fluores-
319 cently labeled neutrophils, macrophages, and *il1β* did not show any difference in comparison to
320 control (**Figure S3c, d, ESI**).

321 When comparing intestinal tissue with body tissue (without intestine) of CuNP exposed
322 embryos, a significant transcriptional upregulation of *il1β* and *irg1l* is measured for the body tis-
323 sue (**Figure 4a**), indicating stronger inflammatory responses in the body or skin cells. In accord-
324 ance with that, confocal imaging of neuromasts on the skin cells revealed a higher expression of
325 *il1β* in all exposures. Remarkably, the strongest signal of *il1β* was found in CuNP exposures, as
326 depicted by increased intensity of the respective GFP tagged line (**Figure 4b**). While the con-
327 trol, Cu(NO₃)₂, and PSNP exposed embryos have healthy skin cells composed by hexagonal
328 cells, the structure is changed in the CuNP exposed embryos, indicating cell death and cell ex-
329 trusion from the epithelium (**Figure 4b, Figure S4a, ESI**). Imaging of the intestines showed that
330 most of the *il1β* positive cells were macrophages surrounding the intestine of CuNP, as well to a
331 minor extent in PSNP, exposed embryos. Close to a neuromast, a cluster of PSNPs was found
332 to be engulfed by an activated macrophage, as it shows *tnfa* expression (**Figure S4b, ESI**).
333 Tissue-specific expression of *irg1l* in the intestinal and dermal epithelium is shown by whole-
334 mount *in situ* hybridization (**Figure 4c**). In some embryos, *irg1l* was strongly expressed in ex-
335 truded cell clusters surrounding the yolk and similar expressional patterns were found for *il1β*
336 (**Figure S5a, b, ESI**) Transcriptional regulation of other genes, assessed by qPCR, is shown in
337 **Figure S6 in the SI**.

338 After injection of 1 nl of 0.5 mg L⁻¹ CuNP and 1 mg L⁻¹ PSNP, transcripts such as *il1β*,
339 *soc3a*, and *ccl20a* were upregulated (**Figure 5a**). In accordance with this, a significantly in-
340 creased neutrophil recruitment in the tail area occurred (**Figure 5b**). PSNP injection did not in-
341 crease neutrophil recruitment. Additional transcriptional changes after injection can be found in
342 **Figure S7** in the ESI.

343 **Discussion**

344 Nanoparticles in an aqueous medium can be taken up by fish in numerous ways and therefore it
345 is expected that initial effects occur at different sites. Here, we assessed dermal and intestinal
346 inflammatory responses to both an inert polystyrene NP (PSNP) and a metal NP (CuNP). Alt-
347 hough our efforts to assess potential inflammatory responses were not exhaustive, NP-specific
348 responses were observed providing preliminary indications that nanoparticles can induce tran-
349 scriptional alteration of pro-inflammatory genes in the skin cells and the tentative gut mucosa,
350 and thus has potential suitability for use in adverse outcome pathways (AOPs).

351 **Nanoparticle contribution to toxicity.** The reactivity and toxicity of nanoparticles are depend-
352 ent on their size in the test medium. Particle size has an inverse effect on the dissolution of
353 metal NPs²⁸ and the smaller the NP the higher the chance of uptake across the cell mem-
354 brane²⁹. As ions are commonly more toxic, it is the ratio between these processes that deter-
355 mine the overall effect. In this study, CuNP clustered to agglomerates in a wide size-range. The
356 agglomeration process is likely to be a dynamic process with small particles ready to contribute
357 to a high dissolution rate and interact with biological surfaces, while bigger agglomerates might
358 conciliate this effect. Thus, while ionic copper is known for inducing hair cell damage and inflam-
359 mation in neuromasts of zebrafish³⁰, the NPs present in the medium might add to this effect. All
360 the three exposures, inert PSNP which remained as single NPs in solution, metallic CuNP, and
361 Cu(NO₃)₂ elicited responses in the endpoints measured here and therefore it is concluded that it
362 is a contribution of both particle and ionic metals.

363 **Innate immune responses in zebrafish skin.** During the first three days of development,
364 zebrafish embryos are protected by a chorionic layer that hampers nanoparticles and to a cer-
365 tain extent also metals from reaching the embryo.^{31–33} In accordance with this, we found that a
366 later stage of embryonic development is more suitable to assess mechanisms of action of nano-
367 particles as the chorion blocks particle and copper passage. After hatching, copper concentra-
368 tions of CuNP exposed embryos were higher than in Cu(NO₃)₂ exposed embryos and PSNP ac-
369 cumulated on the skin, neuromasts, and in the intestine (Figure 2b, Figure 3), indicating an in-
370 creased accumulation of CuNP and PSNP on outer or inner epithelial layers. The gills are not
371 yet functional and the skin cells are enriched with ionocytes (Na⁺-pump-rich cells) taking care of
372 the osmoregulation and therefore transepithelial absorption of ions.³⁴ Although the skin primarily
373 acts as a barrier, it is thus most likely, that the skin epithelium is one of the target organs for
374 NPs or metals released from NPs.

375 With the adaptive immune system not yet being fully developed in zebrafish larvae,³⁵ the
376 innate immunity is their first defense against invaders. Immune responses triggered by NPs is
377 suggested to start with the recognition of the particle by toll-like receptors⁹ or fueled by the NPs
378 generation of free radicals which both can initiate the secretion of cytokines such as *il1β* and
379 *tnfα*. Our data show that *il1β*, was increasingly transcribed in skin cells and neuromasts of all
380 exposed embryos, and in the body (without intestine) samples of CuNP exposed embryos, indi-
381 cating the vulnerability of the outer epithelium. The expression of *il1β* around the neuromast
382 was the most pronounced in CuNP and the membrane-bound *il1β* revealed damaged cellular
383 structure resulting in cell death and cell extrusion from the epithelium (Figure 4b) likely to cause
384 function loss of the neuromasts as shown previously for metal NPs.¹¹ This was less pronounced
385 in Cu(NO₃)₂ and PSNP treated embryos, leading to the conclusion that the response measured
386 for CuNP is a combination of Cu(NO₃)₂ and NP activity. In accordance with this, the number of
387 functional lateral line neuromasts is reduced to a higher extent in CuNP than in CuSO₄ exposed
388 zebrafish embryos (96 hpf)¹¹ and mRNA levels of metallothionein and copper transporter are in-
389 duced more in Cu₂O NP than in CuCl₂ treated zebrafish embryos (120 hpf)³⁶. It is remarkable
390 that plastic NPs elicit an immune response on the epithelial membranes, which has not been re-
391 ported so far. Furthermore, *il1β* is required for the recruitment of neutrophils,²³ which were in-
392 creased in the tail area of at least the CuNP exposed larvae. The results found here are demon-
393 strating consecutive events of a local innate immune responses for CuNP; from adsorption to
394 outer epithelial layers and neuromasts to local induction of pro-inflammatory cytokines to the
395 accumulation of neutrophils.

396 **Innate immune responses in the intestine.** A major target organ for NP accumulation is the
397 intestine, as after hatching, larvae start to open their mouth and transition from yolk to external
398 feeding. Accumulation of NPs in zebrafish larval intestines has been shown previously.³² How-
399 ever, description of local mechanisms of actions is scarce. Özel et al. (2014)³⁷ report increased
400 levels of intestinal serotonin secretion in zebrafish larvae after CuONP exposure, while TiO₂ and

401 As-containing NPs increase intestinal ROS production in zebrafish larvae,^{38,39} and AgNP can
402 disrupt the epithelial mucosa and adversely affect the intestinal microbiota of adult zebrafish⁴⁰.
403 The latter may be related to immune responses as several studies indicate that induction of in-
404 flammation in zebrafish larvae intestines requires the presence of microbes.^{41–43} To our
405 knowledge, we provide the first evidence for gut-associated transcriptional changes of immune
406 response-related genes after NP exposure in zebrafish embryos.

407 In the intestine of exposed zebrafish larvae, an increased local expression of *irg1l* for all
408 exposure groups was found by *in situ* hybridization, which was also hinted by intestinal mRNA
409 expression of CuNP exposed embryos. While a previous *in vitro* study provides evidence that
410 soluble Cu is likely to be responsible for the induction of pro-inflammatory cytokines in intestinal
411 cells,⁴⁴ there is no distinct difference between the intestinal *irg1l* expression of CuNP and
412 Cu(NO₃)₂ treatments in this study (Figure 4c). Moreover, *irg1l* was altered to an even higher ex-
413 tent in body tissue without intestine samples (Figure 4a), indicating the importance of the outer
414 membrane. However, dermal expression of *irg1l* in *in situ* embryos was detected in only a few
415 specimens which might be reasoned with the loss of the loosely attached dermal cells (mucus;
416 Figure S5, ESI) after the repeated washing steps or proteinase K digestion. Both the intestinal
417 as well as the dermal cells are thus sites of action for NPs to induce immune responses. Over-
418 all, taking the expression of *il1β* in intestinal tissue (Figure 4b) into account, responses ap-
419 peared to be weaker in the intestine as compared to the skin cells or neuromasts.

420 Injection of NPs mimics the absorption into the organism which can occur at least for
421 PSNP after waterborne exposure in juvenile zebrafish.⁴⁵ However, the internal concentration of
422 fish in the environment remains speculative. While injection of both CuNP and PSNP in this
423 study led to transcriptional alteration of several immune response-related genes, the number of
424 neutrophils in the tail area was only increased in CuNP injected embryos. Previous studies indi-
425 cated, however, that injected PSNPs can activate pathways related to immune responses when
426 injected into the yolk of 2 days old zebrafish embryos (700 nm PSNPs) as well as in fathead
427 minnow plasma (41 nm PSNP).^{46,47} Because of the complement activation by PSNP⁴⁶, a much
428 earlier response by macrophages could occur, which is not captured after 24 h of exposure in
429 this study or alternatively plastic particles might be ingested by non-immune cells which was
430 exemplified by Hosseini and colleagues⁴⁸.

431 **Innate immune responses in zebrafish as a key event in AOP.** Here we show that different
432 NPs elicit similar inflammatory responses in the tissues affected, particularly the intestine, the
433 skin, and neuromasts. These observations may be of relevance to the efforts to develop com-
434 pound agnostic AOPs, and our data provide potential starting points for such efforts by demon-
435 strating the induction of recognized inflammatory markers. The next steps would be to develop
436 quantifiable assays for the level of induction in order to formalize them as key events, which
437 could be based on standardized microscopy or by transcriptional approaches. Further steps
438 would involve ascertaining the adverse outcome at individual or population levels, as well as the
439 determination of the molecular initiation event which sets off the inflammatory response.

440 In a developing fish, a contaminant-induced stress response will demand energy
441 sources that are otherwise allocated to growth and maintaining overall health. Such adverse
442 outcomes may be initiated by several events (e.g. oxidative stress or inflammation) and can be
443 triggered by various contaminants. To explore the NP-specific effects on overall health and allo-
444 cated energy sources, we compared morphological endpoints such as hatching and growth. No
445 difference between CuNP and Cu(NO₃)₂ was found here, whereas previous results indicate
446 stronger effects on hatching from CuNP than corresponding soluble copper.³³ However, in this
447 study, the detailed confocal imaging of *il1β*, a key player in the inflammatory response, shows
448 clear differences in the two treatments around the neuromasts. Neuromasts are essential to de-
449 tect water movements and thus sense approaching prey, interact socially, or move with the cur-
450 rent (rheotaxis). Several NPs, including TiO₂NP, AgNP, and CuNP as well as soluble copper

451 has the potential to activate apoptotic cell death around lateral line neuromasts and ionocytes
452 which was associated with a reduced ability to orientate in a current.^{11–13,39} It is thus conceivable
453 that NPs accumulating and affecting neuromasts induce behavioral changes as an adverse out-
454 come, which has been reported previously for CuNP⁵⁰, AgNP⁵¹, and PSNP⁵² and was related to
455 neurotoxicity. Our data add to evidence that PSNPs, and likely also CuNPs, accumulate in neu-
456 romasts where they are phagocytosed by macrophages (Figure S4b, ESI), resulting in local in-
457 duction of pro-inflammatory cytokines, which may act as a precursor for damaged or apoptotic
458 neuromasts leading to a potential adverse outcome. Focusing on inflammatory genes here, it is
459 not excluded that oxidative stress plays a role too. A second adverse outcome related to NPs
460 and immune responses may be immunosuppression, as shown by reduced host defense of
461 adult fathead minnows exposed to TiO₂ NPs.⁵³

462 Our data, therefore, suggest key biological target sites for NP exposed fish where an
463 early key event, deregulation of innate immune responsive genes, potentially could lead to an
464 adverse outcome such as a behavioral change. Furthermore, the screening of the neuromasts
465 proved to be a suitable site to detect NP accumulation and inflammatory responses, and there-
466 fore it is suggested that screening of neuromast cells for acute inflammatory response in com-
467 pound toxicity assessments can be extended to nanoparticles. The majority of particles showed
468 adsorption to the outer membranes, specifically in the gut and skin cells and hence caused an
469 acute inflammatory response. As a consequence, the Critical Body Residue approach^{54,55}, al-
470 lowing the relation to the internal accumulation of soluble chemicals to effects, is not applicable
471 for these nanoparticle exposures. Taking the framework of building an Adverse Outcome Path-
472 way¹ is a different approach that allows to mechanistically relate exposure to effects, and can
473 potentially deal with low absorption potential in cells. Our study identifies target tissues of water-
474 borne NP exposure and a set of key players of NP-related molecular effects, the immune
475 marker genes *il1β*, *irg1l*, as well as neutrophil accumulation, suggesting possibilities to relate
476 the induction of inflammatory responses to population-related endpoints. Yet the quantitative re-
477 lationships on dose-responses relativeness of the key events should be determined as a next
478 step. Also, lower concentrations might represent an environmental realistic scenario, although
479 environmental concentrations of particularly nanoplastics are unknown so far.

480 **Conclusions**

481 Using a limited but representative set of inflammatory response markers, this study assessed
482 dermal and intestinal inflammatory responses to both an inert polystyrene NP (PSNP) and a
483 metal NP (CuNP). Obtained results provide the first evidence that nanoparticles can induce pro-
484 inflammatory responses in the skin and intestine cells. Responses were further observed to be
485 more pronounced in the skin, indicating that the skin is more sensitive to NPs than previously
486 anticipated. It can therefore, be speculated that inherent NPs-induced damage to neuromasts
487 embedded in the lateral line can subsequently translate to behavioral changes, and thereby an
488 adverse outcome at the population level. Transcriptional alterations of immune system regulat-
489 ing genes were observed for PSNPs, CuNP, and Cu ions, in which CuNP elicited the strongest
490 response, indicating that both the nanoparticulate form and the metal ion contributed to the ob-
491 served response. The potential of metal and plastic NP to induce innate immune responses in
492 zebrafish embryos thus indicates that this mechanism of action, particularly in the skin, could
493 prove suitable for screening purposes and serve as a building block in AOPs.

494 **Conflicts of interest**

495 There are no conflicts to declare.

496 **Acknowledgements**

497 We would like to thank Redmar Vlieg (Leiden University) for conducting 2-photon microscopy,
498 Roel Heutink (Leiden University) for assistance in NP characterization, Marinda van Pomeran

499 (Leiden University) for assistance in fish experimental work, and Ellard R. Hunting (Leiden Uni-
500 versity) for constructive feedback when writing the manuscript. The staff of the ZF facility of the
501 Cell observatory is thanked for providing the experimental work environment. This study was
502 funded by the Marie Skłodowska-Curie Fellowship (H2020-MSCA-IF-2014-655424) granted to
503 Mónica Varela and the NWO-VIDI 864.13.010 granted to Martina G. Vijver.

504 References

- 505
506 (1) Karcher, S. C.; Harper, B. J.; Harper, S. L.; Hendren, C. O.; Wiesner, M. R.; Lowry, G. V. Visuali-
507 zation tool for correlating nanomaterial properties and biological responses in zebrafish. *Environ.*
508 *Sci. Nano* **2016**, *3*, 1280–1292.
- 509 (2) Ankley, G. T.; Bennett, R. S.; Erickson, R. J.; Hoff, D. J.; Hornung, M. W.; Johnson, R. D.; Mount,
510 D. R.; Nichols, J. W.; Russom, C. L.; Schmieder, P. K.; et al. Adverse outcome pathways: a con-
511 ceptual framework to support ecotoxicology research and risk assessment. *Environ. Toxicol.*
512 *Chem.* **2010**, *29* (3), 730–741.
- 513 (3) Tedesco, S.; Doyle, H.; Blasco, J.; Redmond, G.; Sheehan, D. Oxidative stress and toxicity of gold
514 nanoparticles in *Mytilus edulis*. *Aquat. Toxicol.* **2010**, *100* (2), 178–186.
- 515 (4) George, S.; Lin, S.; Ji, Z.; Thomas, C. R.; Li, L.; Mecklenburg, M.; Meng, H.; Wang, X.; Zhang, H.;
516 Xia, T.; et al. Surface defects on plate-shaped silver nanoparticles contribute to its hazard poten-
517 tial in a fish gill cell line and zebrafish embryos. *ACS Nano* **2012**, *6* (5), 3745–3759.
- 518 (5) Dominguez, G. A.; Lohse, S. E.; Torelli, M. D.; Murphy, C. J.; Hamers, R. J.; Orr, G.; Klaper, R. D.
519 Effects of charge and surface ligand properties of nanoparticles on oxidative stress and gene ex-
520 pression within the gut of *Daphnia magna*. *Aquat. Toxicol.* **2015**, *162*, 1–9.
- 521 (6) van Aerle, R.; Lange, A.; Moorhouse, A.; Paszkiewicz, K.; Ball, K.; Johnston, B. D.; de-Bastos, E.;
522 Booth, T.; Tyler, C. R.; Santos, E. M.; et al. Molecular mechanisms of toxicity of silver nanoparti-
523 cles in zebrafish embryos. *Environ. Sci. Technol.* **2013**, *47* (14), 8005–8014.
- 524 (7) Brun, N. R. N. R.; Lenz, M.; Wehrli, B.; Fent, K. Comparative effects of zinc oxide nanoparticles
525 and dissolved zinc on zebrafish embryos and eleuthero-embryos: Importance of zinc ions. *Sci. To-*
526 *tal Environ.* **2014**, *476–477*, 657–666.
- 527 (8) Khanna, P.; Ong, C.; Bay, B.; Baeg, G. Nanotoxicity: An Interplay of Oxidative Stress, Inflamma-
528 tion and Cell Death. *Nanomaterials* **2015**, *5* (3), 1163–1180.
- 529 (9) Turabekova, M.; Rasulev, B.; Theodore, M.; Jackman, J.; Leszczynska, D.; Leszczynski, J. Immu-
530 notoxicity of nanoparticles: a computational study suggests that CNTs and C60 fullerenes might
531 be recognized as pathogens by Toll-like receptors. *Nanoscale* **2014**, *6*, 3488–3495.
- 532 (10) van Pomeran, M.; Brun, N. R.; Peijnenburg, W. J. G. M.; Vijver, M. G. Exploring uptake and biodis-
533 tribution of polystyrene (nano)particles in zebrafish embryos at different developmental stages.
534 *Aquat. Toxicol.* **2017**, *190* (February), 40–45.
- 535 (11) McNeil, P. L.; Boyle, D.; Henry, T. B.; Handy, R. D.; Sloman, K. a. Effects of metal nanoparticles
536 on the lateral line system and behaviour in early life stages of zebrafish (*Danio rerio*). *Aquat. Toxi-*
537 *col.* **2014**, *152*, 318–323.
- 538 (12) Hernández, P. P.; Moreno, V.; Olivari, F. a.; Allende, M. L. Sub-lethal concentrations of water-
539 borne copper are toxic to lateral line neuromasts in zebrafish (*Danio rerio*). *Hear. Res.* **2006**, *213*
540 (1–2), 1–10.

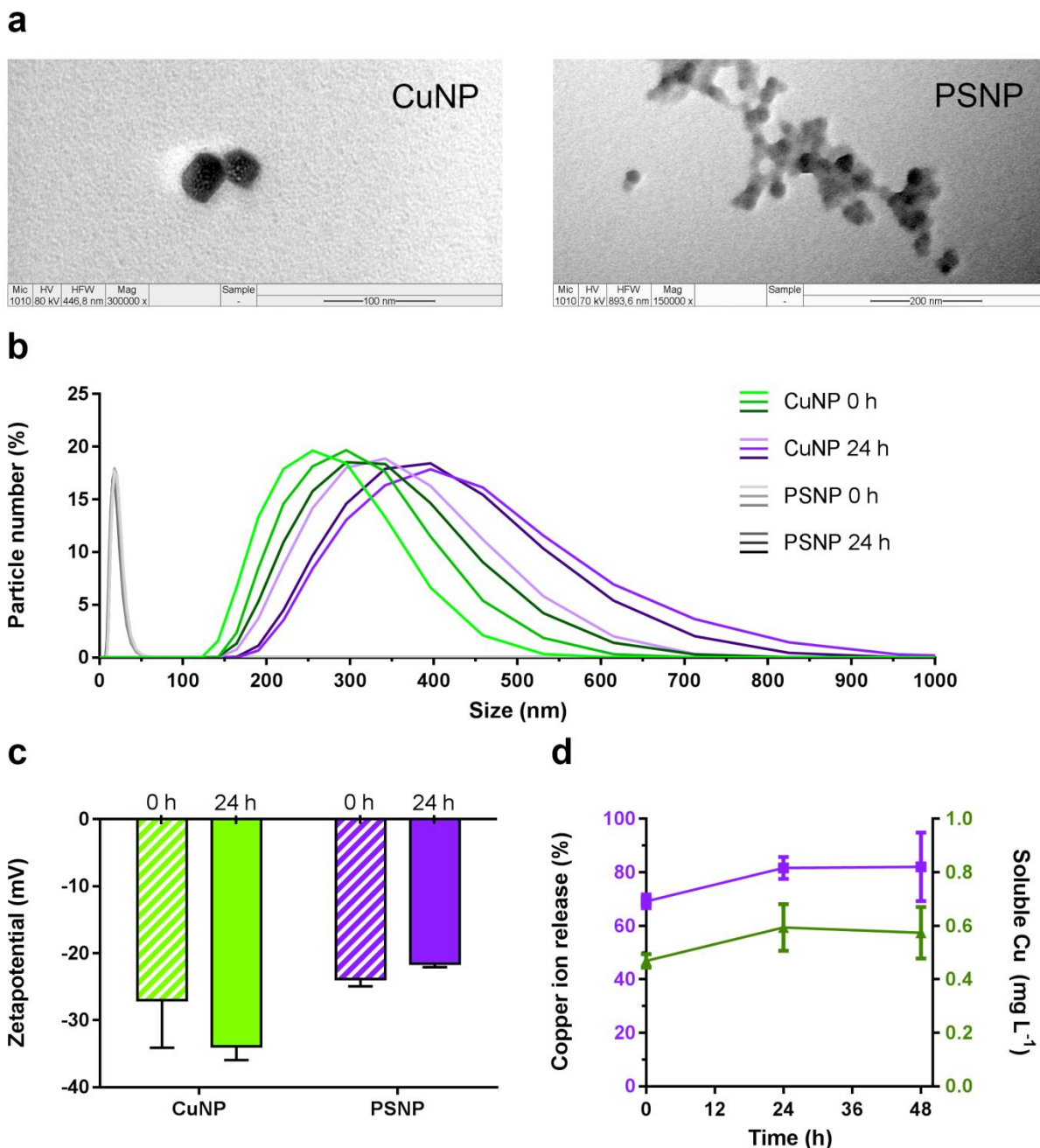
- 541 (13) Osborne, O. J.; Mukaigasa, K.; Nakajima, H.; Stolpe, B.; Romer, I.; Philips, U.; Lynch, I.; Mourabit,
542 S.; Hirose, S.; Lead, J. R.; et al. Sensory systems and ionocytes are targets for silver nanoparticle
543 effects in fish. *Nanotoxicology* **2016**, *10* (9), 1276–1286.
- 544 (14) Wang, T.; Long, X.; Liu, Z.; Cheng, Y.; Yan, S. Effect of copper nanoparticles and copper sulphate
545 on oxidation stress, cell apoptosis and immune responses in the intestines of juvenile *Epinephelus*
546 *coioides*. *Fish Shellfish Immunol.* **2015**, *44* (2), 674–682.
- 547 (15) Truong, L.; Tilton, S. C.; Zaikova, T.; Richman, E.; Waters, K. M.; Hutchison, J. E.; Tanguay, R. L.
548 Surface functionalities of gold nanoparticles impact embryonic gene expression responses. *Nano-*
549 *toxicology* **2013**, *7* (2), 192–201.
- 550 (16) Duan, J.; Yu, Y.; Li, Y.; Li, Y.; Liu, H.; Jing, L.; Yang, M.; Wang, J.; Li, C.; Sun, Z. Low-dose expo-
551 sure of silica nanoparticles induces cardiac dysfunction via neutrophil-mediated inflammation and
552 cardiac contraction in zebrafish embryos. *Nanotoxicology* **2015**, *10* (5), 575–585.
- 553 (17) Renshaw, S. A.; Trede, N. S. A model 450 million years in the making: zebrafish and vertebrate
554 immunity. *Disease Models & Mechanisms* **2012**, *5*(1), 38-47.
- 555 (18) Wang, Z.; Quik, J. T. K. K.; Song, L.; Van Den Brandhof, E.-J. J.; Wouterse, M.; Peijnenburg, W.
556 J. G. M. G. M. Humic substances alleviate the aquatic toxicity of polyvinylpyrrolidone-coated silver
557 nanoparticles to organisms of different trophic levels. *Environ. Toxicol. Chem.* **2015**, *34* (6), 1239–
558 1245.
- 559 (19) Song, L.; Connolly, M.; Fernández-Cruz, M. L.; Vijver, M. G.; Fernández, M.; Conde, E.; de Snoo,
560 G. R.; Peijnenburg, W. J. G. M.; Navas, J. M. Species-specific toxicity of copper nanoparticles
561 among mammalian and piscine cell lines. *Nanotoxicology* **2014**, *8* (4), 383–393.
- 562 (20) Gustafsson, J.P., 13 September 2015. Visual MINTEQ Version 3.1. Stockholm, Sweden.
563 <https://vminteq.lwr.kth.se/>. (Accessed 20 January 2017).
- 564 (21) Lawson, N. D.; Weinstein, B. M. In vivo imaging of embryonic vascular development using trans-
565 genic zebrafish. *Dev Biol* **2002**, *248* (2), 307–318.
- 566 (22) Ellett, F.; Pase, L.; Hayman, J. W.; Andrianopoulos, A.; Lieschke, G. J. mpeg1 promoter
567 transgenes direct macrophage-lineage expression in zebrafish. *Blood* **2011**, *117* (4), e49-56.
- 568 (23) Nguyen-Chi, M.; Phan, Q. T.; Gonzalez, C.; Dubremetz, J.-F.; Levraud, J.-P.; Lutfalla, G. Transi-
569 ent infection of the zebrafish notochord with *E. coli* induces chronic inflammation. *Dis. Model.*
570 *Mech.* **2014**, *7* (7), 871–882.
- 571 (24) Nguyen-Chi, M.; Laplace-Builhe, B.; Travnickova, J.; Luz-Crawford, P.; Tejedor, G.; Phan, Q. T.;
572 Duroux-Richard, I.; Levraud, J. P.; Kissa, K.; Lutfalla, G.; et al. Identification of polarized macro-
573 phage subsets in zebrafish. *Elife* **2015**, *4* (JULY 2015), 1–14.
- 574 (25) Abramoff, M. D.; Magalhães, P. J.; Ram, S. J. Image Processing with ImageJ. *Biophotonics Int.*
575 **2004**, *11* (7), 36–42.
- 576 (26) Thisse, C.; Thisse, B. High-resolution *in situ* hybridization to whole-mount zebrafish embryos. *Nat.*
577 *Protoc.* **2008**, *3* (1), 59–69.
- 578 (27) Koch, B. E. V; Stougaard, J.; Spaink, H. P. Spatial and temporal expression patterns of chitinase
579 genes in developing zebrafish embryos. *Gene Expr. Patterns* **2014**, *14*, 69–77.
- 580 (28) Zhai, Y.; Hunting, E. R.; Wouterse, M.; Peijnenburgh, W. J. G. M.; Vijver, M. G. Importance of ex-
581 posure dynamics of metal-based nano-ZnO, -Cu and -Pb governing the metabolic potential of soil
582 bacterial communities. *Ecotoxicol. Environ. Saf.* **2017**, *145*, 349-358.

- 583 (29) Zhu, M.; Nie, G.; Meng, H.; Xia, T.; Nel, A.; Zhao, Y. Physicochemical properties determine nano-
584 material cellular uptake, transport, and fate. *Acc. Chem. Res.* **2013**, 46(3), 622-631.
- 585 (30) d'Alençon, C. A.; Peña, O. A.; Wittmann, C.; Gallardo, V. E.; Jones, R. A.; Loosli, F.; Liebel, U.;
586 Grabher, C.; Allende, M. L. A high-throughput chemically induced inflammation assay in zebrafish.
587 *BMC Biology* **2010**, 8:151.
- 588 (31) Fent, K.; Weisbrod, C. J.; Wirth-Heller, A.; Pieleles, U. Assessment of uptake and toxicity of fluores-
589 cent silica nanoparticles in zebrafish (*Danio rerio*) early life stages. *Aquat. Toxicol.* **2010**, 100 (2),
590 218–228.
- 591 (32) van Pomeran, M.; Brun, N. R.; Peijnenburg, W. J. G. M.; Vijver, M. G. Exploring uptake and biodis-
592 tribution of polystyrene (nano)particles in zebrafish embryos at different developmental stages.
593 *Aquat. Toxicol.* **2017**, 190, 40–45.
- 594 (33) Muller, E. B.; Lin, S.; Nisbet, R. M. Quantitative Adverse Outcome Pathway Analysis of Hatching
595 in Zebrafish with CuO Nanoparticles. *Environ. Sci. Technol.* **2015**, 49, 11817–11824.
- 596 (34) Jänicke, M.; Carney, T. J.; Hammerschmidt, M. Foxi3 transcription factors and Notch signaling
597 control the formation of skin ionocytes from epidermal precursors of the zebrafish embryo. *Dev.*
598 *Biol.* **2007**, 307 (2), 258–271.
- 599 (35) Trede, N. S.; Langenau, D. M.; Traver, D.; Look, A. T.; Zon, L. I. The use of zebrafish to under-
600 stand immunity. *Immunity* **2004**, 20 (4), 367–379.
- 601 (36) Chen, D., Zhang, D., Yu, J. C., & Chan, K. M. Effects of Cu₂O nanoparticle and CuCl₂ on zebrafish
602 larvae and a liver cell-line. *Aquat. Toxicol.* **2011**, 105(3–4), 344–54.
- 603 (37) Ozel, R. E.; Wallace, K. N.; Andreescu, S. Alterations of intestinal serotonin following nanoparticle
604 exposure in embryonic zebrafish. *Env. Sci Nano* **2014**, 2014 (1), 27–36.
- 605 (38) Osborne, O. J.; Lin, S.; Jiang, W.; Chow, J.; Chang, C. H.; Ji, Z.; Yu, X.; Lin, S.; Xia, T.; Nel, A. E.
606 Differential effect of micron- versus nanoscale III–V particulates and ionic species on the zebrafish
607 gut. *Environ. Sci. Nano* **2017**, 4 (6), 1350–1364.
- 608 (39) He, X.; Aker, W. G.; Hwang, H.-M. An *in vivo* study on the photo-enhanced toxicities of S-doped
609 TiO₂ nanoparticles to zebrafish embryos (*Danio rerio*) in terms of malformation, mortality, rheo-
610 taxis dysfunction, and DNA damage. *Nanotoxicology* **2014**, 8, 185–195.
- 611 (40) Merrifield, D. L.; Shaw, B. J.; Harper, G. M.; Saoud, I. P.; Davies, S. J.; Handy, R. D.; Henry, T. B.
612 Ingestion of metal-nanoparticle contaminated food disrupts endogenous microbiota in zebrafish
613 (*Danio rerio*). *Environ. Pollut.* **2013**, 174, 157–163.
- 614 (41) He, Q.; Wang, L.; Wang, F.; Li, Q. Role of Gut Microbiota in a Zebrafish Model with chemically in-
615 duced enterocolitis involving toll-like receptor signaling pathways. *Zebrafish* **2014**, 11 (3), 255–
616 264.
- 617 (42) Oehlers, S. H.; Flores, M. V.; Hall, C. J.; Crosier, K. E.; Crosier, P. S. Retinoic acid suppresses
618 intestinal mucus production and exacerbates experimental enterocolitis. *Dis. Model. Mech.* **2012**,
619 5 (4), 457–467.
- 620 (43) Brugman, S. The zebrafish as a model to study intestinal inflammation. *Dev. Comp. Immunol.*
621 **2016**, 64, 82–92.
- 622 (44) Piret, J.-P.; Vankoningsloo, S.; Mejia, J.; Noël, F.; Boilan, E.; Lambinon, F.; Zouboulis, C. C.; Ma-
623 sereel, B.; Lucas, S.; Saout, C.; et al. Differential toxicity of copper (II) oxide nanoparticles of simi-
624 lar hydrodynamic diameter on human differentiated intestinal Caco-2 cell monolayers is correlated
625 in part to copper release and shape. *Nanotoxicology* **2012**, 6 (7), 789–803.

- 626 (45) Skjolding, L. M.; Ašmonaitė, G.; Jølck, R. I.; Andresen, T. L.; Selck, H.; Baun, A.; Sturve, J. Assessment of the importance of exposure route for uptake and internal localization of fluorescent
627 nanoparticles in zebrafish (*Danio rerio*) using light sheet microscopy. *Nanotoxicology* **2017**, *11* (3),
628 351–359.
629
- 630 (46) Veneman, W. J.; Spaink, H. P.; Brun, N. R.; Bosker, T.; Vijver, M. G. Pathway analysis of systemic
631 transcriptome responses to injected polystyrene particles in zebrafish larvae. *Aquat. Toxicol.* **2017**,
632 *190* (July), 112–120.
- 633 (47) Greven, A. C.; Merk, T.; Karagöz, F.; Mohr, K.; Klapper, M.; Jovanović, B.; Palić, D. Polycarbonate
634 and polystyrene nanoplastic particles act as stressors to the innate immune system of fathead
635 minnow (*Pimephales promelas*). *Environ. Toxicol. Chem.* **2016**, *35* (12), 3093–3100.
- 636 (48) Hosseini, R., Lamers, G. E. M., Soltani, H. M., Meijer, A. H., Spaink, H. P., & Schaaf, M. J. M. Ef-
637 ferocytosis and extrusion of leukocytes determine the progression of early mycobacterial patho-
638 genesis. *Journal of Cell Science* **2016**, *129* (18), 3385-3395.
- 639 (49) Hua, J.; Vijver, M. G.; Ahmad, F.; Richardson, M.; Peijnenburg, W. J. G. M. Toxicity of different-
640 sized copper nano- and submicron particles and their shed copper ions to zebrafish embryos. *En-
641 viron. Toxicol. Chem.* **2014**, *33*(8), 1774-1782.
- 642 (50) Sun, Y.; Zhang, G.; He, Z.; Wang, Y.; Cui, J.; Li, Y. Effects of copper oxide nanoparticles on devel-
643 oping zebrafish embryos and larvae. *Int. J. Nanomedicine* **2016**, *11*, 905–918.
- 644 (51) Garcia-Reyero, N.; Kennedy, A. J.; Escalon, B. L.; Habib, T.; Laird, J. G.; Rawat, A.; Wiseman, S.;
645 Hecker, M.; Denslow, N.; Steevens, J. a.; et al. Differential effects and potential adverse outcomes
646 of ionic silver and silver nanoparticles *in vivo* and *in vitro*. *Enviromental Sci. Technol.* **2014**, *48*,
647 4546–4555.
- 648 (52) Chen, Q.; Gundlach, M.; Yang, S.; Jiang, J.; Velki, M.; Yin, D.; Hollert, H. Quantitative investiga-
649 tion of the mechanisms of microplastics and nanoplastics toward zebrafish larvae locomotor activ-
650 ity. *Sci. Total Environ.* **2017**, *584–585*, 1022–1031.
- 651 (53) Jovanović, B.; Whitley, E. M.; Kimura, K.; Crumpton, A.; Palić, D. Titanium dioxide nanoparticles
652 enhance mortality of fish exposed to bacterial pathogens. *Environ. Pollut.* **2015**, *203*, 153–164.
- 653 (54) Barron, M. G.; Anderson, M. J.; Lipton, J.; Dixon, D. G. Evaluation of critical body residue QSARS
654 for predicting organic chemical toxicity to aquatic organisms. *SAR QSAR Environ. Res.* **1997**, *6*
655 (1–2), 47–62.
- 656 (55) McCarty, L. S.; Arnot, J. A.; Mackay, D. Evaluation of critical body residue data for acute narcosis
657 in aquatic organisms. *Environ. Toxicol. Chem.* **2013**, *32* (10), 2301–2314.

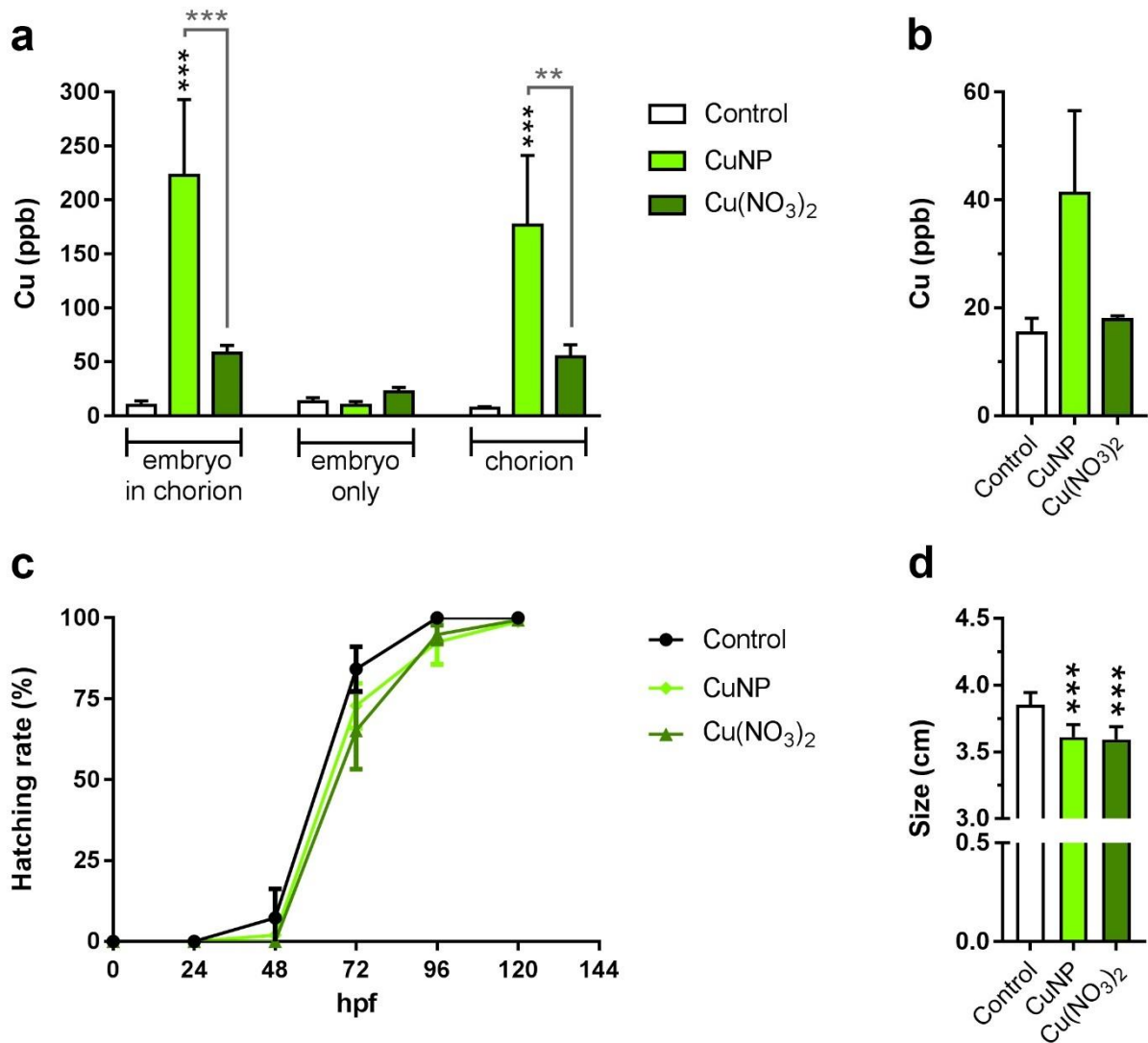
658

659



660
 661 **Figure 1. Characterisation of CuNP and PSNP in exposure medium.** (a) TEM image of 25 nm CuNP in egg water supplemented
 662 with SRHA (Scale bar: 100 nm) and of 25 nm PSNP in egg water (Scale bar: 200 nm) after 1 h of incubation. NP agglomerates in
 663 TEM images are not representative of what was found in the majority of the pictures but represents the picture with the best contrast
 664 to derive shape and size. (b) DLS profile showing the distribution of the hydrodynamic diameter of CuNP in egg water supplemented
 665 with SRHA and PSNP in egg water after 0 h and 24 h. (c) Zeta potential of CuNP and PSNP after 0 h and 24 h. (d) Dissolution pro-
 666 file of Cu over time of 1 mg L⁻¹ CuNP in egg water supplemented with SRHA at different time points in % and mg L⁻¹. Error bars are
 667 + standard deviation (SD) of measured values for each exposure group consisting of 3 replicates.

668
 669

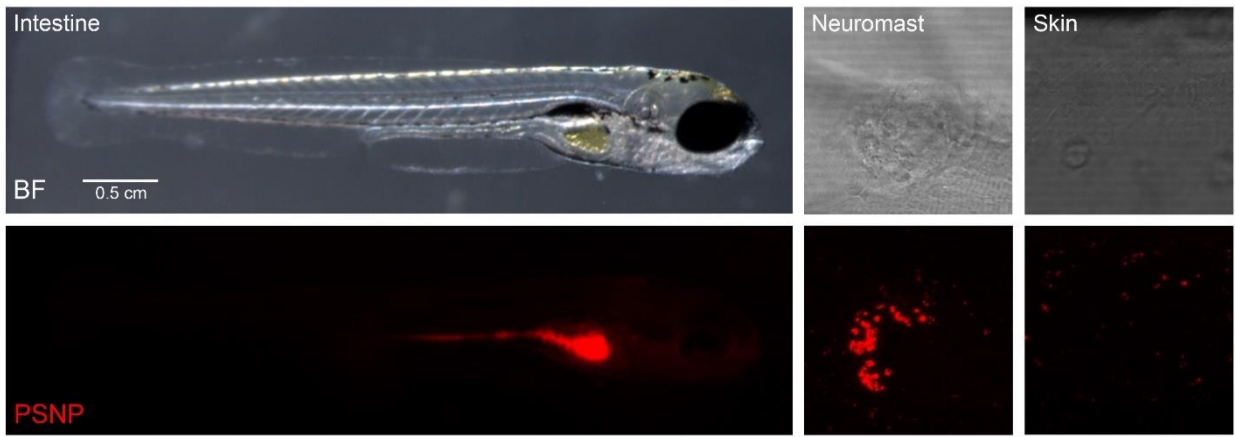


670
 671 **Figure 2. Effects of CuNP and corresponding Cu(NO₃)₂ exposure on zebrafish embryo development.** Zebrafish embryos were
 672 exposed to 1 mg L⁻¹ CuNP and corresponding Cu(NO₃)₂ concentration (0.59 mg L⁻¹) from 0-120 hpf. (a) Total copper concentration
 673 in zebrafish embryos, dechorionated embryos, and chorions in µg per embryo at 72 hpf and (b) total copper concentration in
 674 zebrafish embryos at 120 hpf (n = 3). (c) Hatching rates of zebrafish embryos demonstrating equally delayed hatching success of
 675 zebrafish embryos exposed to CuNP and Cu(NO₃)₂ (n = 5, with 10 embryos per replicate). (d) Effect of 1 mg L⁻¹ CuNP and corre-
 676 sponding Cu(NO₃)₂ on growth of zebrafish embryos measured as body length at 120 hpf (n = 10). Error bars are + standard devia-
 677 tion (SD) of measured values for each exposure group.

678

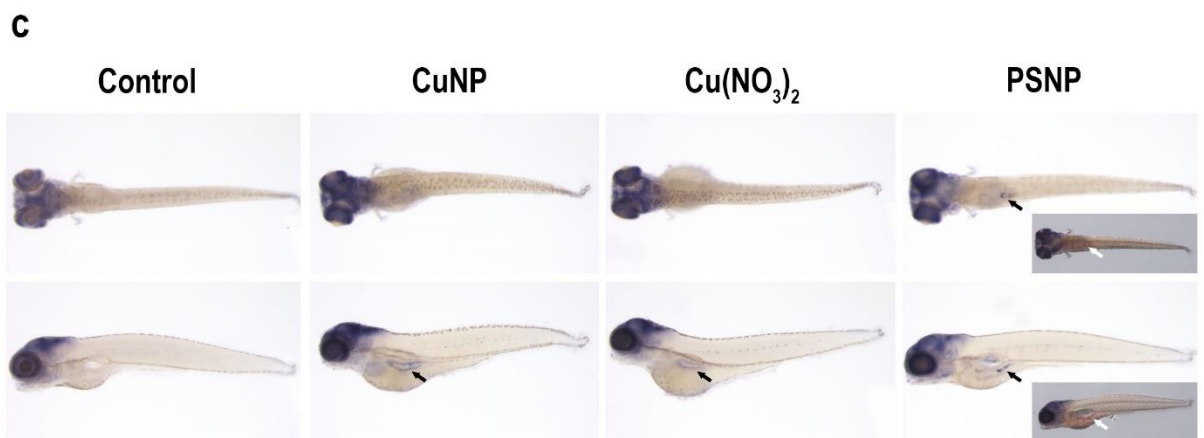
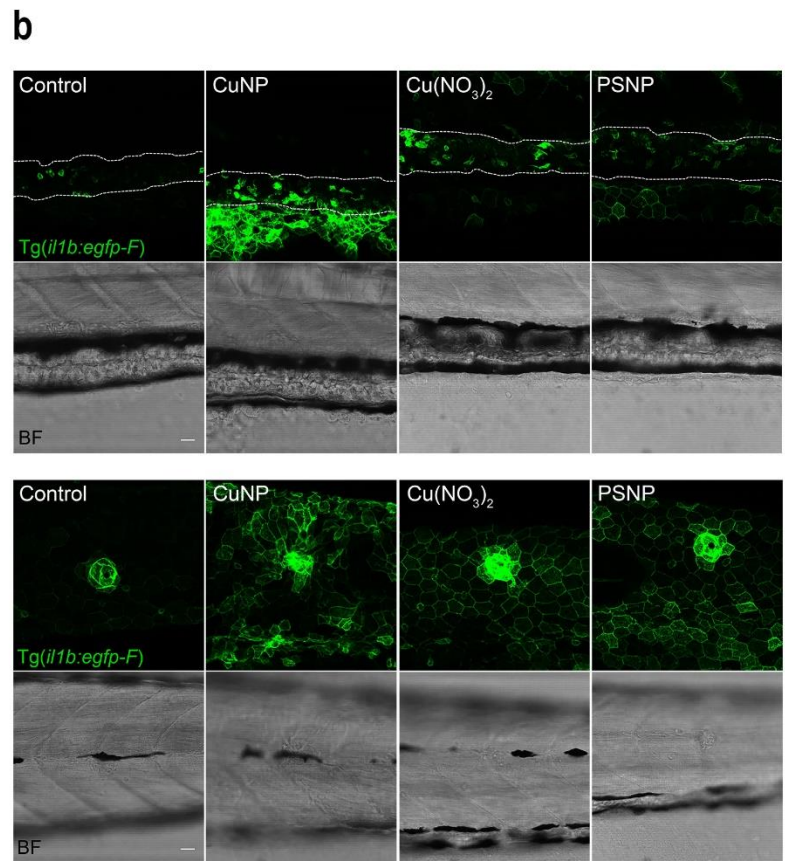
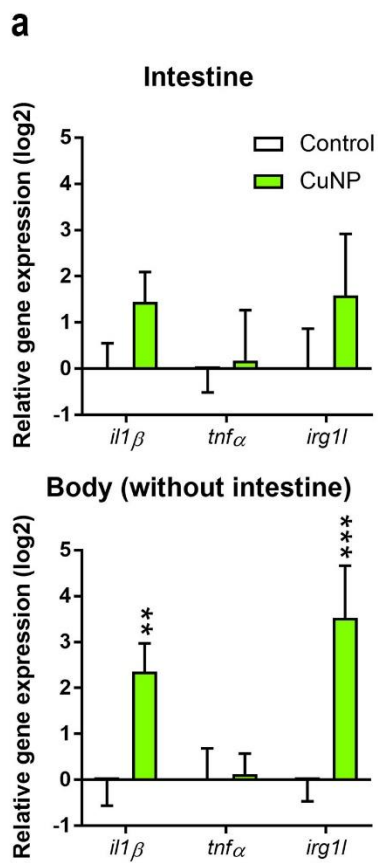
679

680

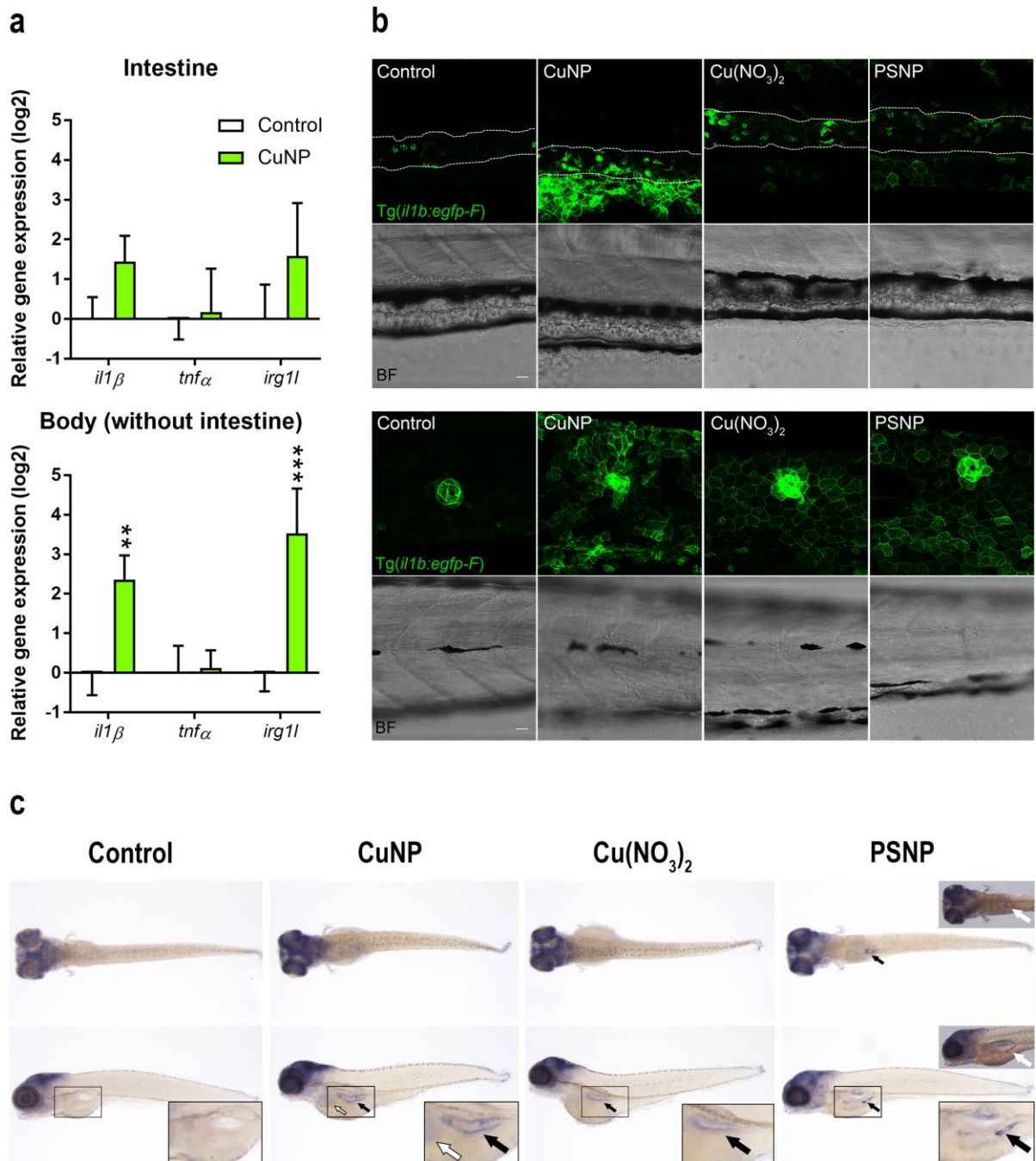


681
682 **Figure 3. Main target organs of PSNP accumulation in zebrafish embryo at 120 hpf.** Representative fluorescence microscopy
683 image depicting accumulation of PSNP (red) in the intestine and confocal microscopy images depicting PSNP accumulation in the
684 cavity of a neuromast on the lateral line and skin (tail).

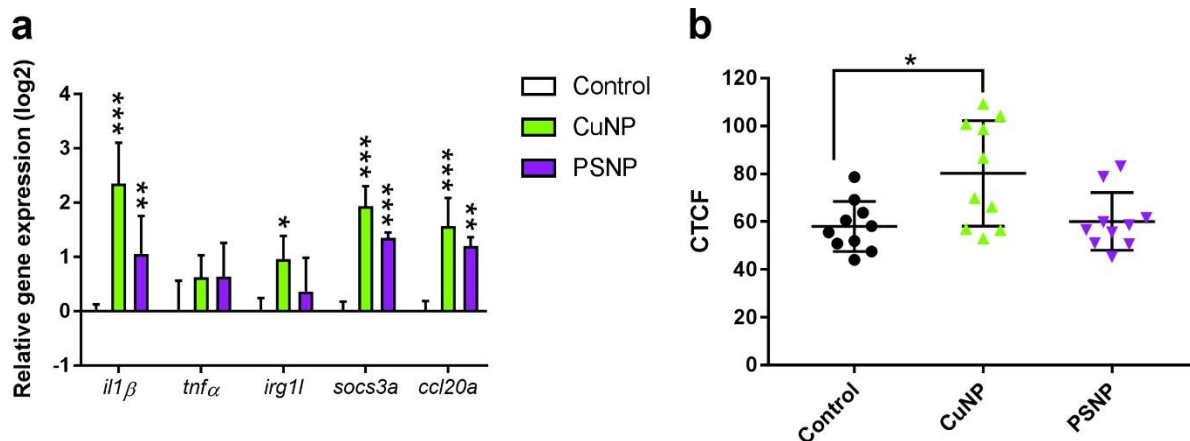
685



686



687
 688 **Figure 4. Local expression of immune response regulated genes in embryonic intestine and skin after waterborne expo-**
 689 **sure from 72-120 hpf. (a)** Transcriptional alterations of immune response related genes (*il1β*, *irg1l*, *tnfa*) in intestinal tissue and
 690 body tissue without intestine of wild-type zebrafish embryos exposed to 1 mg L⁻¹ CuNP. Relative expression levels were normalized
 691 to *rpl13a*, calculated relative to expression levels in control embryos. Asterisks indicate significant differences to controls (*p < 0.05,
 692 **p < 0.01, and ***p < 0.001). Values are presented as mean ± SD (n = 3). (b) Representative images of caudal intestines (above)
 693 and neuromasts (below) of control with SRHA, 1 mg L⁻¹ CuNP, corresponding Cu(NO₃)₂, and 10 mg L⁻¹ PSNP waterborne exposed
 694 *Tg(il1b:eGFP-F)* embryos. Egg water control and SRHA control were similar. The transgenic reporter zebrafish line *Tg(il1b:eGFP-F)*
 695 expresses a membrane-targeted green fluorescent protein (GFP-F) under the control of the interleukin 1 beta (*il1β*) promoter. White
 696 lines delineate the intestine. CuNP exposed embryos display non-hexagonal shaped cells. Scale bars = 20 μm. (c) Representative
 697 images of *in situ* hybridization showing the expression profile of *irg1l* mRNA in wild-type zebrafish embryos after exposure to 1 mg L⁻¹
 698 CuNP, corresponding Cu(NO₃)₂ concentration, and 10 mg L⁻¹ PSNP from 72-120 hpf. For PSNP exposure group a fluorescent mi-
 699 croscope picture is inserted showing the presence of fluorescent particles (red; white arrow) in the intestine. Strongest staining was
 700 observed in the intestine after exposure to either CuNP, Cu(NO₃)₂, and PSNP (black arrow).



702

703 **Figure 5. Inflammatory responses in zebrafish embryos after injection of CuNP and PSNP.** (a) Transcriptional alterations of
 704 immune response related genes (*il1β*, *tnfa*, *irg1l*, *socs3a*, *ccl20a*) in zebrafish embryos injected with 1 nl of 1 nl of 0.5 mg L⁻¹ CuNP
 705 and 1 mg L⁻¹ PSNP at 30 hpf and sampled 54 hpf. Relative expression levels were normalized to *rp113a*, calculated relative to ex-
 706 pression levels in control embryos. Values are presented as mean ± SD (n = 5). (b) Corrected total cell fluorescence (CTCF) of the
 707 tail area from *Tg(mpx:eGFP)* zebrafish embryos, in which GFP is expressed in neutrophils, injected with CuNP and PSNP at 30 hpf
 708 and imaged at 54 hpf. Values are presented as mean ± SD (n = 10). Asterisks indicate significant differences to controls (*p < 0.05,
 709 **p < 0.01, and ***p < 0.001).